NJC

PAPER

Cite this: *New J. Chem.*, 2019, 43, 15201

A Raman, SERS and UV-circular dichroism spectroscopic study of *N*-acetyl-L-cysteine in aqueous solutions†

R. A. Cobos Picot,[a] M. Puiatti,[b] A. Ben Altabef,[a] R. J. G. Rubira,[c] S. Sanchez-Cortes,[d] S. B. Diaz[a] and M. E. Tuttolomondo *[a]

Received 10th May 2019,
Accepted 19th August 2019

DOI: 10.1039/c9nj02427a

rsc.li/njc

The aim of this work is to evaluate the vibrational and structural properties of *N*-acetyl-L-cysteine (NAC), and its molecular structure and electronic properties in relation to the action of thiol and amine groups at different pH. Raman and Surface Enhanced Raman Spectroscopy (SERS) spectra were measured in aqueous solution. The influence of an aqueous environment on the NAC spectra was simulated by means of an implicit (polarizable continuum model) method. SERS spectra indicate that the S atom is interacting with the surface through the sulfur atom. One of the consequences of the interaction with the surface is the deprotonation of the SH group, as revealed by the disappearance of the ν(S–H) band. The calculations performed for the Ag–NAC complex confirm the experimental data obtained by SERS, where the S–Ag interaction is the most important. These results are very interesting when one can formulate the drug feasibility of NAC using silver nanoparticles as a carrier. Raman spectra were measured to compare the behavior of different functional groups in the molecule, both in the solid phase and in aqueous solution at different pH. Apparent ionization constants (pK' values) for the S–H group at high ionic strengths were calculated from the intensity of the 2580 cm^{-1} frequency as a function of pH. UV and circular dichroism spectra were also measured in aqueous solution at different pH. Finally, the study was completed with natural bond orbital (NBO) analysis to determine the presence of hyper-conjugative interactions. It is important to observe the behavior of the C2–N bond with the delocalization effect; as the pH increases the hyperconjugative interaction of this bond decreases in the same way as in the case of νCN. The way in which the LP πO1 → σ*C2–N interaction and νCN decrease is an inverse reflection of the fractional ionization α_{SH}.

1. Introduction

The aim of the present work is to evaluate the electronic, vibrational and structural properties of *N*-acetyI-L-cysteine and its electronic behavior in relation to the action of NAC reactive groups at different degrees of solvation and pH.

The thiol or sulfhydryl groups in cysteine residues have attracted a great deal of attention because of their ability to take part in a variety of biological reactions. The role of the thiol group as a possible hydrogen-bond donor and acceptor has been explored in a number of studies.[1,2] *N*-Acetl-L-cysteine (NAC) is a derivate of cysteine, the only natural occurring amino

[a] *INQUINOA-CONICET, Instituto de Química Física, Facultad de Bioquímica, Química y Farmacia, Universidad Nacional de Tucumán, San Lorenzo 456, T4000CAN, Tucumán, Argentina. E-mail: metuttolomondo@fbqf.unt.edu.ar*
[b] *INFIQC – CONICET, Instituto de Investigaciones en Físico-Química Orgánica de Córdoba, – Facultad de Químicas, Universidad Nacional de Córdoba, Córdoba, Argentina*
[c] *São Paulo State University (UNESP), School of Technology and Applied Sciences, 19060-900, Presidente Prudente, SP, Brazil*
[d] *Instituto de Estructura de la Materia, IEM-CSIC, Serrano 121, 28006 Madrid, Spain*

† Electronic supplementary information (ESI) available: Free energies (energies in Hartrees), differences in free energies for three conformers of *N*-acetyl cisteine (Table S1); experimental and calculated bond distances and angles for NAC (Table S2); free energies (energies in Hartrees), differences in free energies for three conformers of NACdep (Table S3); calculated bond distances and angles for NACdep (Table S4); selected bands observed in the Raman and SERS spectra of *N*-acetyl-L-cisteine in aqueous solution at different pH (Table S5); free energies (energies in Hartrees), differences in free energies for three conformers of NACdepp (Table S6); calculated bond distances and angles for NAC-depp (Table S7); selected bands observed in the Raman spectra of *N*-acetyl-L-cisteine in aqueous solution at 6.93–12 pH (Table S8); pK' values of the –SH group in NAC (Table S9); The pH metric titration curve of NAC (Fig. S1); Raman spectra of NAC in the solid state and in water solution at different concentrations (Fig. S2); fractional ionization α_{SH} *vs.* concentration (Fig. S3); calculated potential curves for the Ag–S bond (up) and Ag–O (down) in $NACdep^-$ using semiempirical (PM6) levels of theory (Fig. S4); calculated potential curves for the Ag–S bond (up) and Ag–O (down) in 3-$NACdep^-$ using semiempirical (PM6) levels of theory (Fig. S5); theoretical UV spectra of the $NACdepp^{2-}$ form in water solution (Fig. S5); Raman spectra of NAC at different pH values in the 1500–1200 region (Fig. S6). See DOI: 10.1039/c9nj02427a

acid with a reactive sulfhydryl group. The S–S group is able to fix the secondary structure of the proteins and, therefore, act as a stabilizing element of the structure.[3] NAC is a commercially available drug; the reducing action of NAC also explains the mucolytic activity due to the effect of NAC in reducing heavily cross-linked mucus glycoproteins, a breaking effect on disulphides and the ability to restore thiol pools, which in turn regulates the redox state. *N*-Acetyl-cysteine is an antioxidant whose effect has been extensively studied in experimental animal models, especially related to the oxidative stress generated by pesticides.[4–8]

The *N*-acetylcysteine reduced thiol is a precursor of L-cysteine and can serve as a precursor for glutathione synthesis, a potent antioxidant that eliminates free radicals and reactive oxygen species (ROS). The ability of *N*-acetylcysteine to increase intra and extracellular glutathione can be a crucial factor in renal tissue protection in nephropathies induced by contrast media.[9,10] NAC is undoubtedly the best known booster of intracellular glutathione (GSH).[11] *In vitro* research indicates that NAC is able to stimulate glutathione biosynthesis. *In vitro*, NAC increases intracellular glutathione levels in erythrocytes and liver cells and lungs and restores the stock glutathione that had experimentally been reduced. In humans, oral NAC supplementation normalizes low glutathione levels; GSH concentrations were increased 20% in the skin and 50% in the liver after one dose of 1200 mg kg^{-1} NAC, whereas lung and kidney GSH were unaffected.[11] It acts as a biosynthetic precursor of most endogenous antioxidants that participate in the disintegration of peroxides.[12] Besides, NAC has protective effects against mitochondrial injury and apoptosis started by oxidant stimulants *in vitro*.[12,13]

The crystal structure of NAC was determined at room temperature by X-ray (T – 295 K) and neutron diffraction (T – 16 K) methods by Fusao Takusagawa and Thomas F. Koetzle.[14] Boeckx *et al.*[15] conducted a theoretical study of the conformational properties of NAC and compared these results with an experimental study of NAC isolated in an argon matrix at 16 K. Afterwards, Poopari and colleagues published a theoretical and experimental study (IR and VCD, vibrational circular dichroism) on the corresponding stretching modes of amide groups I and C=O of the dominant conformations of *N*-acetyl-L-cysteine methyl ester and NAC in water.[16]

The calculation of the ionization constants of amino and thiol groups in cysteine from experimental titration data has given rise to considerable controversy. R. Cecil gives a good brief summary in a review.[17] Several investigators have formulated their results in terms of a set of microscopic constants.[18,19] Reported studies on the Raman spectra of two sulfhydryl compounds, thioglycolic acid and cysteine, involve quantitative determination of the intensities and polarization of the Raman bands. The apparent ionization constants, pK' values, of the sulfhydryl group were calculated through pH changes in the intensity of the S–H stretching frequency near 2580 cm^{-1}.

In Scheme 1 a route from deprotonation of NAC at different pH is presented. The molecule that we will call NAC lies between pH 1 and 2.5 in its acid form. Deprotonation of the COOH group starts at pH 2.5 (the deprotonated NAC is called NACdep$^-$ (CO_2^-)). It should be noted that both species coexist between pH 2.5 and 3. Deprotonation of the thiol group (SH) begins at pH 6.14, forming a dianion called NAC depp^{-2} (S^-).

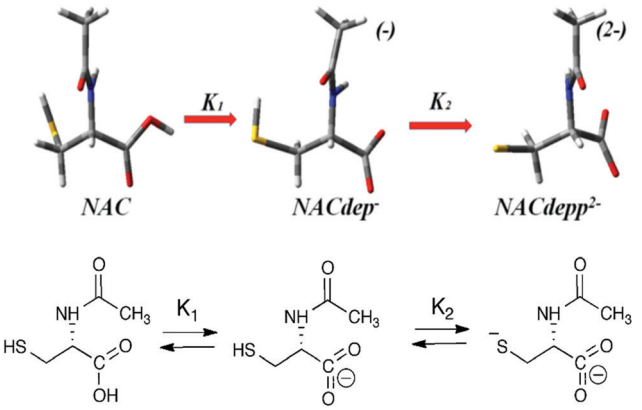

Scheme 1 NAC deprotonation route at different pH.

Raman and SERS spectra were measured to compare the behavior of different functional groups in the molecule, both in the solid phase and in aqueous solution at different pH. The results of SERS indicate that there are two possible types of interaction: carboxylate and SH, where the fundamental interaction is verified with the C–S group. These vibrational results were confirmed with those obtained theoretically, and have remarkable potential interest in the formulation of NAC-based drugs using silver nanoparticles as a carrier.

Thiol pK' values are key behavior indicators of the thiol group reactivity and functionality. Raman spectra of NAC in different states of ionization are reported, with quantitative determination of the intensities of the Raman bands using a Raman spectrometer. In this paper, we report a Raman-based pH method that enables reliable quantification of thiol pK' values. The degree of thiol ionization is monitored directly using the peak intensity of the S–H stretching feature in the 2580 cm^{-1} region relative to an internal reference peak as a function of the solution's pH.

UV-dichroism measurements were performed at different pH. These were used to determine which of the conformations are present in the measured deprotonation states.

Thus, the fully optimized geometry was obtained for NAC, NACdep$^-$ and NACdepp^{-2} using different combinations of theoretical methods and basis sets, in the isolated state and in water solution. In order to explain the behavior of bioavailable sites in aqueous solution, calculations were performed including the solvent. The influence of an aqueous environment on the NAC spectra was simulated by means of implicit medium, where the solvent is described as continuous, dielectric or conductor-like (IEF-PCM model). Calculations in continuous solvent are of interest to explain the behavior of bioavailable sites in this medium.[20–24] In order to characterize the behavior of NAC on silver nanoparticles theoretical calculations were performed, simulating a molecule with two silver atoms attached to NAC. The results helped us to complement experiments and provide important information which could corroborate what was seen experimentally. Moreover, natural bond orbital (NBO)[25,26] analysis was performed to determine the presence of hyper-conjugative interactions.

2. Materials and methods

Samples of *N*-acetyl-L-cysteine (NAC; $HSCH_2CH(NHCOCH_3)$-CO_2H, M_W = 163.19 g mol^{-1}) were purchased from Sigma-Aldrich. Its purity was confirmed by spectroscopy.

2.1 Raman spectroscopy

The Raman dispersion spectrum of the solid was measured in the 3500–200 cm^{-1} interval with a Thermo Scientific DXR Raman microscope. Water solutions of NAC at different concentrations (from 1 M to 2×10^{-2} M) and different pH were measured with a Thermo Scientific DXR Smart Raman spectrometer. The solid sample was placed on gold-coated sample slides and the liquid sample was placed in a glass cuvette. To achieve a sufficient signal to noise ratio, 100 acquisitions of 2 seconds each were performed during the measurements with the laser power maintained at 10 mW. Raman data were collected using a diode-pump, a solid state laser of 532 nm (5 cm^{-1} spectral resolution), a confocal aperture of a 25 μm pinhole and a 10× objective.

2.2 Method for pK' calculation of sulfhydryl dissociation

A pH metric curve of NAC to more alkaline pH was obtained with NaOH 0.1 M solution measured with a pH meter Mettler Toledo MP220 (Fig. S1, ESI†).

The S–H stretching frequency of thiol compounds in the Raman spectrum is sharp and very intense. The band centered at 2580 cm^{-1} in the Raman spectrum of the saturated water solution (1 M) is assigned to the S–H stretching mode.

The intensity of this band is important to ascertain the degree of ionization of the thiol group at different pH. This study was carried out following the procedure proposed by Elson and Edsall[19] for cysteine. We considered two strong bands in particular: the S–H stretching band at ∼2580 cm^{-1} and the C–S stretching band at ∼686 cm^{-1}. The intensity of the latter appears to be independent of the concentration and pH and therefore it serves as a convenient internal standard for determining the relative intensity of the 2580 cm^{-1} band as it decreases with decreased concentration of dilutions (increasing the pH). At a pH 6 value, where we may assume the sulfhydryl group to be un-ionized, the peak height ratio is $I_{SH}/I_{CS} = 2.00 \pm 0.01$. We denote this ratio as A_0, and the others as A. Then, the fractional ionization of the S–H group, αS–H, may be taken as:

$$\alpha_{SH} = 1 - (A/A_0). \quad (1)$$

The ratio I_{SH}/I_{CS} may be taken as a measure of α_{SH}, the fractional ionization of the sulfhydryl group, and the pK' value may thus be calculated from the expression:

$$\mathrm{pH} = \mathrm{p}K' + \log\frac{\alpha_{SH}}{(1-\alpha_{SH})} \quad (2)$$

2.3 SERS spectra

Silver nitrate ($AgNO_3$, M_W = 169.88 g mol^{-1}), hydroxylamine hydrochloride ($NH_2OH{\cdot}HCl$, M_W = 69.49 g mol^{-1}), sodium hydroxide (NaOH, M_W = 40.00 g mol^{-1}), sodium chloride (NaCl, M_W = 5844 g mol^{-1}) and potassium nitrate (KNO_3, M_W = 101 1032 g mol^{-1}) (all of analytical grade) were purchased from Merck and Sigma-Aldrich. Absolute ethanol of analytical grade (99.5% purity) was also obtained from Merck. Stock solutions of these substances were prepared in ethanol at a concentration of 0.1 M and were further diluted when necessary.

Raman spectra were obtained using a micro-Raman inVia Renishaw spectrograph, equipped with an electrically cooled CCD camera, and a Leica DM 2500 microscope, under 532 nm excitation, and a diffraction grating of 1800 L mm^{-1}. The laser power reaching the sample was about 2.0 mW and the spectral resolution was set to 2 cm^{-1}. The 532 nm line provided by an Nd–YAG laser (Samba model, Cobolt) was used as an excitation source. The integration time of the measurements was 10 sec.

Hydroxylamine AgNPs (AgH) were employed to obtain the SERS spectra. Briefly, 10 mL of a 10^{-2} M silver nitrate solution was added dropwise to 90 mL of a 1.6×10^{-3} M solution of hydroxylamine hydrochloride adjusted to pH = 9 under vigorous stirring. The resulting spherical AgNPs had an average size of 35 nm in diameter.[27] All aqueous solutions needed for preparation of the metal colloids were prepared using Milli-Q water (18.2 MΩ cm resistivity).

The enhancement factor can be calculated according to the following expression:

$$E_f = I_{SERS} \times c_{sol}/I_{sol} \times c_{SERS}$$

where I_{SERS} is the intensity of the SERS spectrum band; c_{sol} is the concentraction of the water solution; I_{sol} is the intensity of the regular Raman spectrum of the same band; and c_{SERS} is the concentration of NAC used to obtain the SERS spectrum.

2.4 UV circular dichroism spectroscopy

The circular dichroism spectra were collected with a J-815 circular dichroism and UV/vis absorbance spectrometer for solutions at 10^{-3} M at pH values of 3, 5 and 10 with a path length of 1 mm.

2.5 Theoretical methods

Quantum chemistry calculations were performed using the Gaussian 03 and 09 programs.[28,29] In order to find relevant conformers of NAC in solution, an exploration was performed with the V Conf program by using molecular mechanics. Geometry optimization was achieved for all conformers obtained from this search using the Density Functional Theory (DFT) hybrid functional B3LYP[30,31] with the 6-311++G(d,p) basis set within the polarizable continuum model (IEF-PCM)[32] to account for solvent effects on the isomerism. All calculations were spin restricted and of the frozen-core type. The vibration wavenumbers were calculated from both numeric and analytic second derivatives to confirm that the optimized structures corresponded to minima on the potential-energy surface (PES). Experimental frequencies were compared with the ones calculated at the B3LYP/6-311++G(d,p) level for all atoms.

The Ag–NACdep$^-$ interaction was analyzed by performing a previous geometry optimization followed by vibrational frequency calculations. The calculations were performed on the isolated molecule using the B3LYP hybrid functional in combination with

the LanL2DZ effective core potential basis set[33] for the Ag atom and the 6-311++G(d,p) basis set[34,35] for C, N, O, S and H atoms. The Ag–NACdep$^-$ complex was treated as an open-shell system using spin unrestricted DFT wavefunctions (UB3LYP).

The atomic displacements, represented graphically by means of the program GaussView,[36] were used to describe the normal modes.

Natural bond orbital (NBO) calculations[37] were performed at the B3LYP/6-311++G(d,p) level using the NBO 3.0 code as implemented in Gaussian 03.

3. Results

3.1 Analysis of NAC at pH 1.79–2.5

Previous studies revealed that the carboxylic group in NAC exists essentially as –COOH at pH = 2.5, and as COO$^-$ at pH = 7.0, whereas both species coexist at pH = 3.1.[38]

We performed a stochastic exploration of the PES to find the most stable structure in aqueous solution for this pH region, taking into account the relevant conformational degrees of freedom. From this search, accomplished with molecular mechanics, 9 geometries were obtained and their electronic energy minima computed with DFT at the B3LYP/6-31G(d) level in continuous solvent (SCRF calculations). The conformations within 8 kJ mol^{-1} of the most stable one were selected for further refinement with DFT at the B3LYP/6-311++G(d,p) level also in continuous solvent. As a result, four different conformations characterized as local minima were obtained (Fig. 1 and Table S1, ESI†).

Several inter and intra molecular hydrogen bonds were reported by means of X-ray (T = 295 K) and neutron (T = 16 K) diffraction studies.[14] In these interactions the thiol group acts both as a donor and acceptor, being involved in the S–H···O and N–H···S interactions. They show an intramolecular N–H···O contact similar to that found here as observed in many amino acids, *e.g.* α-glycine.[39] The thiol group is involved in short contacts with the carbonyl O of the carboxyl group and with the N atom, and the N···S and H···S distances were determined in the room temperature X-ray diffraction study.

Some geometric parameters calculated for the four most stable conformers found within the implicit solvent model are presented in Table S2 (ESI†). Only conformer 2-NAC has a favorable orientation in aqueous solution for the formation of a hydrogen bond type N–H···O3 like that reported in the structure of the solid.[14] All intramolecular hydrogen bonds in aqueous solution where the thiol group is involved were not observed.

Vibrational properties. The bands observed in the solid state and water solution Raman spectra were interpreted in terms of the NAC normal modes of vibration. A tentative assignment of bands was assisted by the calculated conformations and their frequency modes and from comparison with spectra of related amino acids, especially cysteine (Table S3, ESI†).[40–43]

Since the relative sensitivity of the Raman equipment makes it necessary to work at relatively high concentrations, we only dealt with concentrations higher than 0.02 M up to 1 M. Fig. S2 (ESI†) shows the spectra of the most representative dilutions. The calculated spectra for the most stable conformers found within implicit solvent with an approximate description of some vibrational modes are presented in Fig. 2.

The two bands observed at 1718 and 1590 cm^{-1} in the solid state Raman spectrum were assigned to the C═O$_{acid}$ (carboxylic group) and C═O$_{acetyl}$ (amide group) stretching modes (Fig. S1, ESI†). These bands appear at 1723 and 1641 cm^{-1} in the water solution Raman spectrum (Fig. 2) because the hydrogen atom H of the carboxyl group forms a bond with the O(1) (acetyl oxygen) of a neighboring molecule in the solid phase; when NAC is in solution this hydrogen bond is broken and the force constant of the C═O$_{acetyl}$ group increases, leading to an upward shift of the corresponding wavenumbers. The intensity of the C═O acid band decreases as the concentration of the solution is lowered, with an increase of the C–O intensity. This is reflected in the shift observed in the band at 1228 cm^{-1} (corresponding to the C–O stretching mode) from the solid to 1135–1128 cm^{-1} in solution, in agreement with the calculations (Fig. S2, ESI†).

Koetzel[14] reports that the thiol group acts as an acceptor and a donor group through hydrogen bonds, as seen by the behavior of υSH. The band centered at 2548 cm^{-1} in the Raman spectrum of the solid is assigned to the S–H stretching mode. This band appears at higher wavenumbers (2580 cm^{-1}) in the Raman

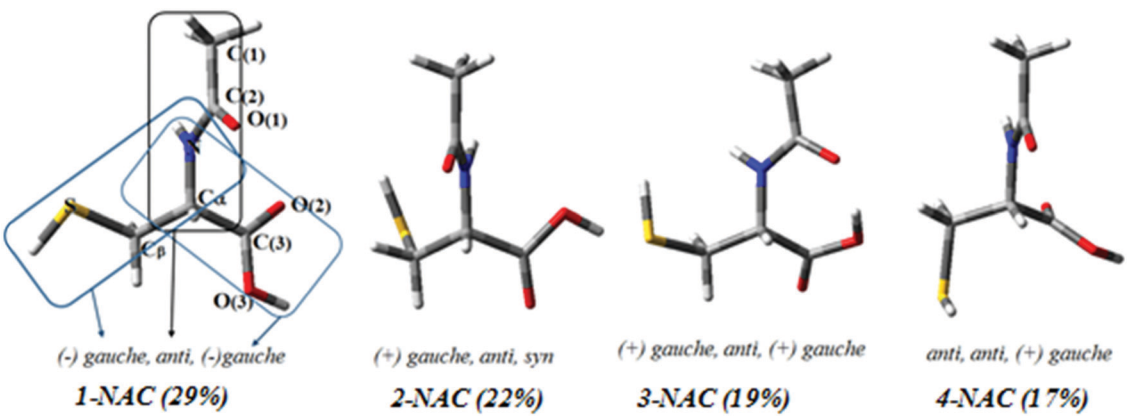

Fig. 1 Four different conformations of NAC characterized as local minima obtained with B3LYP/6-311++G(d,p).

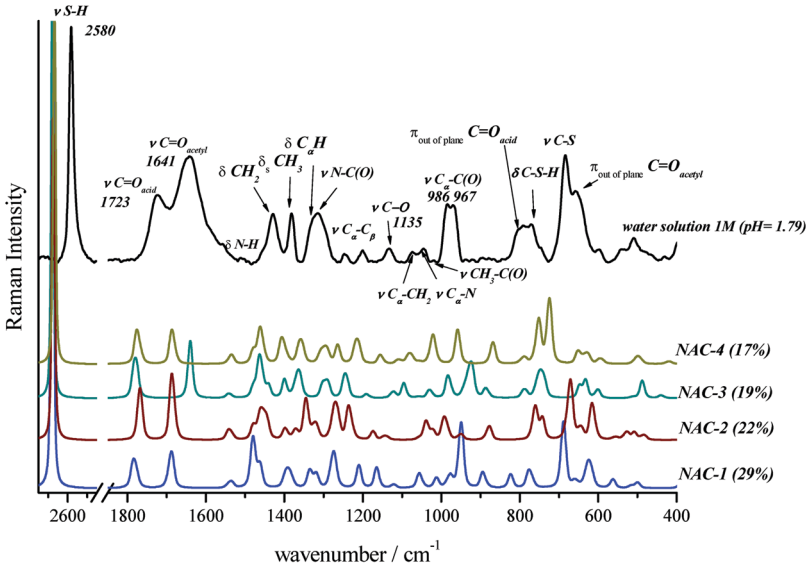

Fig. 2 Experimental Raman spectra of NAC in water solution (above) and calculated spectra of four NAC conformers at the B3LYP/6-311++G(d,p) level (below).

spectrum of NAC in solution because the solvation of the solid breaks the intermolecular hydrogen bond between the H of the SH group and the lone pair of the N and O (in the C═O_{acetyl} group). This band is sensitive to dilution and it may be seen to shift to higher wavenumbers when the concentration decreases. In Fig. S3 (ESI†) we show α_{SH} (fractional ionization) as a function of concentration. The degree of ionization varies in the 0–0.30 interval and α_{SH} decreases with decreasing concentration because of the range of concentrations dealt with here. This is consistent with the increased frequency observed in the SH stretching band. Hence, only the unionized form of the thiol group can be detected at the analyzed pH.

The band located at 989 cm^{-1} in the spectrum of the solid shows a split and a shift to lower frequencies in the spectrum of the aqueous solution. This band corresponds to the νC_α–C(O) mode. Therefore, these modes are overlapped in the solid state. In contrast, in aqueous solution two intense bands are observed at 986–967 cm^{-1}. This is because the 1-NAC and 3-NAC conformations are present in aqueous solution (Fig. 2).

3.2 Analysis of NAC at pH 2.5–6.14

We calculated the deprotonated form following the same procedure previously described for NAC and obtained five conformations. Only three had a difference of 3 kJ mol^{-1} in free energy (ΔG) (Fig. 3 and Table S4, ESI†). At this range of pH NAC is deprotonated: ($NACdep^-$), since COOH has become the COO^- group.

An intramolecular bond between the amide group H and O of the COO^- group is observed in the three conformers. The intramolecular hydrogen bond between the H of the SH group and the N of amide I occurs only in the 2-$NACdep^-$ conformer (Table S5, ESI†).

In order to better analyze the results of the SERS spectrum, a study of the Ag–1-$NACdep^-$ (*gauche* form) and Ag–$NACdep^-$ (*anti* form) interactions was performed. To do this, the potential energy barrier was calculated based on the distances Ag–S (thiol group) and Ag–O (carboxylic group). This calculation was performed by using the PM6 semi-empirical method for the Ag–*gauche* and Ag–*anti* complex (Fig. S4 and S5, ESI†). The optimized molecular structure calculated at the B3LYP level is shown in Fig. 4.

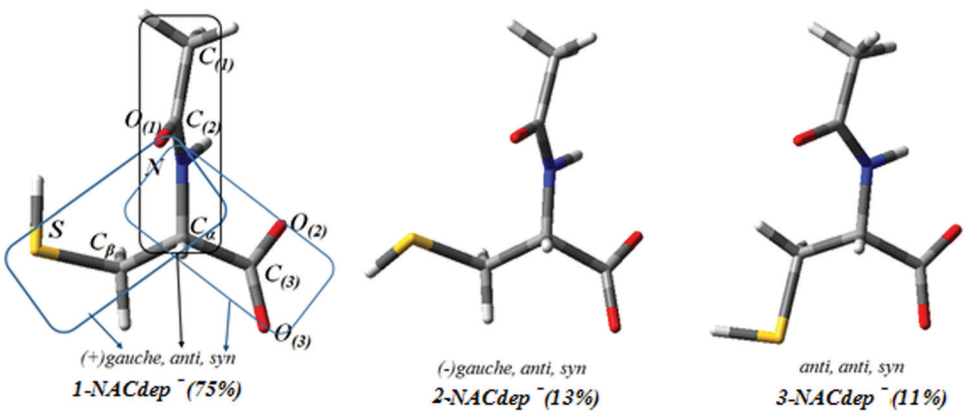

Fig. 3 Three different conformations of $NACdep^-$ characterized by local minima obtained with B3LYP/6-311++G(d,p).

It can be observed that the most stable interaction occurs when the Ag atom is close to the S atom of NACdep$^-$. In addition, the closer the metal atom to the carboxylic group, the more unstable the Ag–NACdep$^-$ complex. Another interesting fact is that the closer the Ag atom to the SH group, the longer the S–H distance becomes, leading finally to the thiolate form.

Vibrational properties. Fig. 4 shows the Raman spectra of NAC present in saturated aqueous solution (1 M) in a pH range between 2.5 and 6.14. According to the literature, protonated and deprotonated NAC coexist in the pH range between 2.5 and 3. This can be seen by checking the intensity of the stretch C═O$_{acid}$ band seen at 1721 cm^{-1}, which undergoes a clear intensity decrease as the pH is increased and disappears completely at pH 4.1. This change occurs simultaneously with the emergence of bands assigned to the CO_2^- group symmetric and antisymmetric stretches, which appear as a consequence of the deprotonation of the carboxylic group. These bands can be seen above pH 3.0 as shoulders at 1558 and 1395 cm^{-1}. Above pH 4.01 these symmetric stretching bands have medium intensity. In addition, a well-defined band at 820 cm^{-1} attributed to the bending mode of the group CO_2^- is observed at pH above 4.01.

The band assigned to the N–C(O) stretching motion in the amide group also undergoes an intensification and shift from 1313 cm^{-1}, at pH 1.79, to 1296 cm^{-1} at pH 6.14. In this pH range the thiol group (SH) undergoes no change in aqueous solution. The SH stretching band that appears in the solid state at 2548 cm^{-1} moves to a higher frequency at 2581 cm^{-1} in aqueous solution because in the solid state this group is forming intermolecular H-bonds and behaves both as a donor (N–H(N)$\cdots$S) and acceptor (H(S)$\cdots$O).[14] The C–S stretching band appears at 686 cm^{-1} and remains unchanged at different pH. The CSH deformation appears as a broad band from pH 2 to pH $>$ 4.01 and it becomes a medium intensity band at 780 cm^{-1} with pH 5.10.

SERS spectra of NAC were obtained on silver colloids in order to compare them with the Raman spectra in solution and to evaluate the conformational changes occurring when interacting with a metal surface. We calculate the intensification factor only if the intensities of normal Raman and SERS are similar, giving a value of about 10^6 for concentrations in solutions of 1 M and 2 μM. SERS spectra of Cys were already studied on Au and Ag nanoparticles and different conformations were deduced from the analysis of these spectra.[36] SERS spectra were measured at different concentrations (Fig. 5) and a steric effect was observed at higher concentrations. Fig. 6 shows the SERS spectra of NAC (25 μM) on Ag metal colloids, normal Raman and Raman calculated for three conformers.

The SERS spectrum of NAC (Fig. 5) provides useful information concerning molecule adsorption on the metal. The strong bands at 1377 and 948 cm^{-1}, assigned to the symmetric $\nu(CO_2^-)$ and ν(Cα–CO_2^-), and the strong downward shift of the $\nu(CO_2^-)$ band as compared to that observed in the aqueous phase ($\sim$1395 cm^{-1}, Fig. 5 and Table S3, ESI†) suggest a interaction of carboxyl groups with the metal surface. On the other hand, the high intensity of the 1281 cm^{-1} band, assigned to the νN–C(O) vibration, together with the red shift of ν(Cα–N) at 1089 cm^{-1}, brings us to the conclusion that the NH of the amide group could also be involved in the interaction with the surface or remain relatively close to the surface.

The most striking change occurring in the SERS spectrum is the splitting of the strong C–S stretching band, which appears in the normal Raman spectrum (pH 6.00 at 685 cm^{-1}) in two bands at 735 and 650 cm^{-1}. It indicates that the S atom is interacting with the surface through the sulfur atom. One of the consequences of the interaction with the surface is the deprotonation of the SH group, as revealed by the disappearance of the ν(S–H) band (which appears at 2581 cm^{-1} in solution, Fig. 6). In order to facilitate the interaction of the COO$^-$ and CS groups with the metal, the NAC molecule is oriented on the surface favoring the presence of 1-NACdep$^-$(*+g,a,s*) and 3-NACdep$^-$(*a,a,s*) conformers leading to the reinforcement of the band at 735 cm^{-1}. A similar result was found in the case of Cys[41] although in the latter case a weaker CS band was seen at higher wavenumbers (or frequencies). This difference is attributed to the acetyl residue linked to the amino group, which may induce a higher steric impediment.

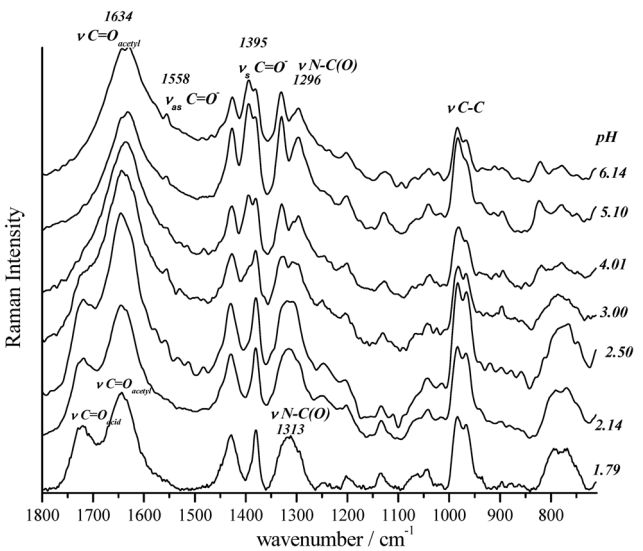

Fig. 4 Raman of NAC (1 M) water solution at different pH values.

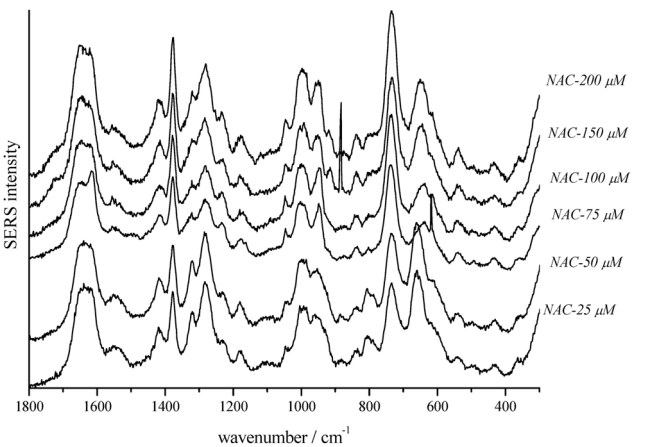

Fig. 5 SERS spectra of NAC at different concentrations.

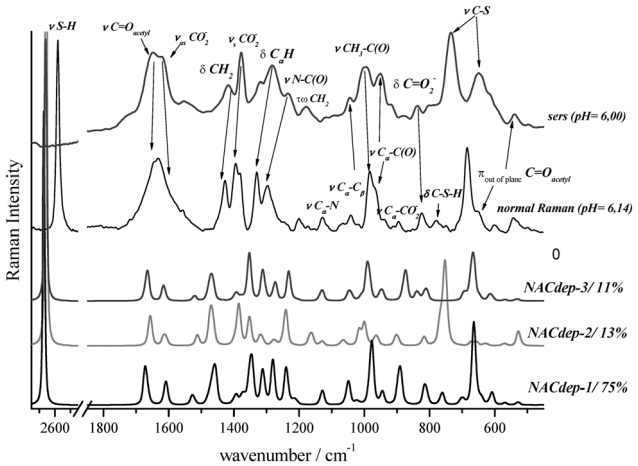

Fig. 6 SERS spectra of NAC (25 μM) on Ag metal colloids, normal Raman and Raman calculated for the three conformers.

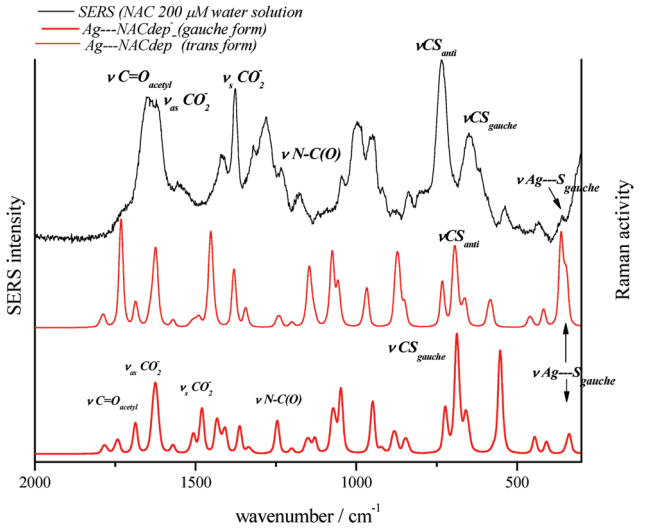

Fig. 7 SERS spectra of NAC (200 μM) on Ag metal colloids, and Raman calculated for Ag–1-NACdep$^-$ (*gauche* form) and Ag–3-NACdep$^-$ (*anti* form).

Upon analysis of the SERS spectra we have deduced that the Ag–S interaction seems to be the most important in the adsorption of NAC onto the metal surface; the interaction with COO^- is not as fundamental here, since as a consequence of the interaction with SH we can have a conformational change that affects the bands of C═O_{amide}, CN and Cβ/Cα.

The two C–S bands observed at 735 cm^{-1} and 648 cm^{-1} are attributed to the *anti* and *gauche* forms, respectively. The C–S stretching band appears at lower frequencies for the gauche conformer, while the band at 1380 cm^{-1} is attributed to the symmetrical stretching mode of the COO^-, whose intensity slightly changes between both conformations. The *anti* form appears more intense at high concentrations (Fig. 5 and 6) and implies a greater degree of order in the adsorbed chains. However, the *gauche* form increases at low concentrations, when structural change is more likely to facilitate a joint approach of CS and COO^- to the metal. This observation was confirmed by the spectrum calculated for the interaction of 1–3NACdep$^-$ with Ag (Fig. 7).

3.3 Analysis of NAC at pH 6.14–12

The deprotonation of the thiol group (SH) is observed spectroscopically in this pH range.

The S–H stretching frequency of thiol compounds in the Raman spectrum is sharp and very intense (in the infrared spectrum it is relatively weaker). In aliphatic thiols it lies in the 2570–2580 cm^{-1} region, which is virtually free of other Raman bands. The changes of pH in the intensity of the S–H stretching frequency near 2580 cm^{-1} allow the calculation of the apparent p*K* values of the sulfhydryl group.

The band centered at 2580 cm^{-1} in the Raman spectrum of the saturated water solution (1 M) is assigned to the S–H stretching mode (Table S8, ESI†). This band decreases in intensity as the pH increases, because of the deprotonation of the SH group (S^-). In the 6–10 pH range, the two species of NAC:NACdep$^-$ and NACdepp^{-2} have the acid site (CO_2^-) deprotonated and the beginning of SH group deprotonation may be observed. Thus, only the ionized form of the thiol group (S^-) can be observed in the aqueous solution at pH 12.

In this pH range, quantum calculations were performed for NAC depp^{-2} (S^-) form. To do this, a conformational search was conducted by means of molecular dynamics calculations of the molecule. Three stable conformations were found, 1-NACdepp^{-2}, 2-NACdepp^{-2} and 3-NACdepp^{-3}, with a respective population of 42%, 38% and 13% (Table S6, ESI†).

Fig. 8 shows the conformations with their contribution of population and symmetry. The conformers with symmetry +*g* are the most populated. Intramolecular hydrogen bonds are present in the three conformers. In 1-NACdepp^{-2} the orientation of the amide and C–S groups favors the formation of the hydrogen bond, N–H···S. In the case of the 2-NACdepp^{-2} and 3-NACdepp^{-3} conformers, the hydrogen bond is formed by the interaction of the H atom of the amide group H and the O of the COO^- group (Table S7, ESI†).

The deprotonation of the NACdep$^-$ SH group leads to the coexistence of NACdepp^{-2} and NACdep$^-$ up to pH 11.30. In Fig. 9 the Raman spectrum of NAC is presented from pH 6.93 to pH 12.

Fig. 10 shows the Raman spectrum of a NAC saturated solution (1 M) to pH 12 and the Raman spectra calculated with B3LYP/6-311++G(d,p). We present the most probable assignment of the main modes of NACdepp^{-2} shown. The Raman spectra calculated for the 1-NACdepp^{-2} and 2-NACdepp^{-2} conformers are those that resemble the experimental spectrum, but spectroscopic observation is not possible.

Fig. 11 shows the variation of α_{SH} against pH. Note that for the range of pH studied here, the degree of ionization varies in the 0–1.0 interval and α_{SH} decreases with decreasing pH.

The pK' value obtained for 1 M NACdepp^{-2}, 9.54, is an average value from the last column of Table S9 (ESI†). This value is in accordance (pK = 9.5) with those reported in the literature.[44]

The NAC pK' value is higher than those reported for cysteine by Benesch and Benesch (1955),[45] E. L. Elson and J. T. Edsall (1961)[19] and Reuben and Bruice (1976),[46] which were 8.53, 8.50 and 8.21 respectively.

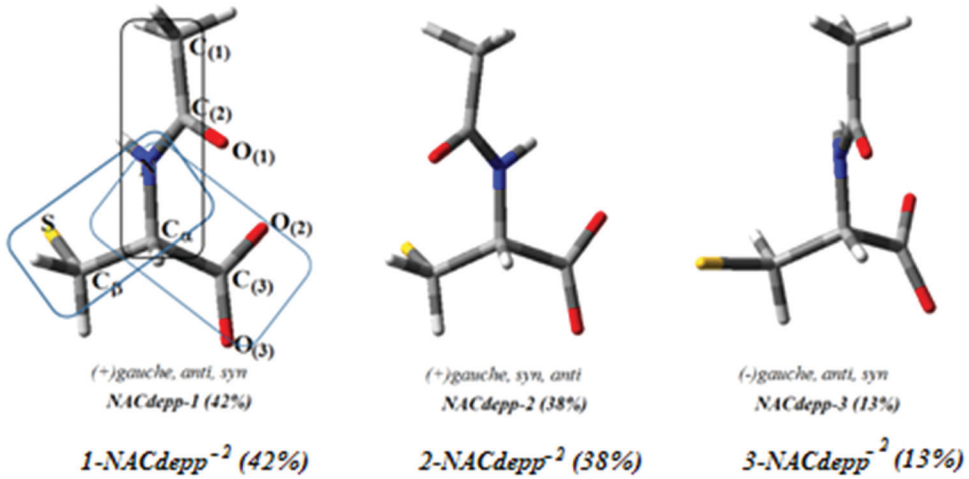

Fig. 8 Three different conformations for NACdepp^{-2} characterized as local minima obtained with B3LYP/6-311++G(d,p).

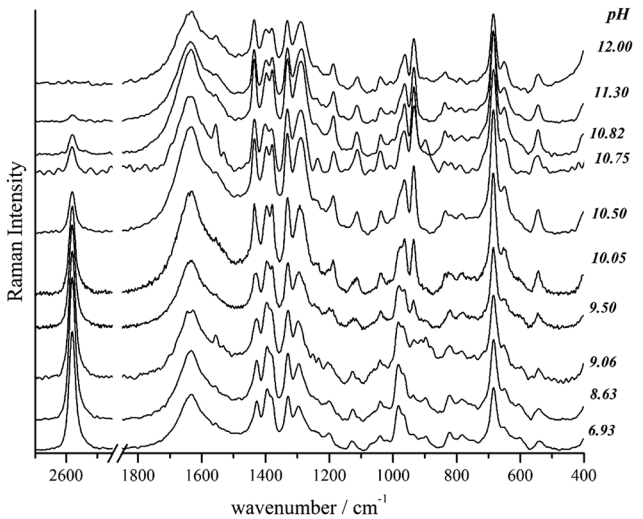

Fig. 9 Raman of the water solution of NAC (1 M) at different pH values.

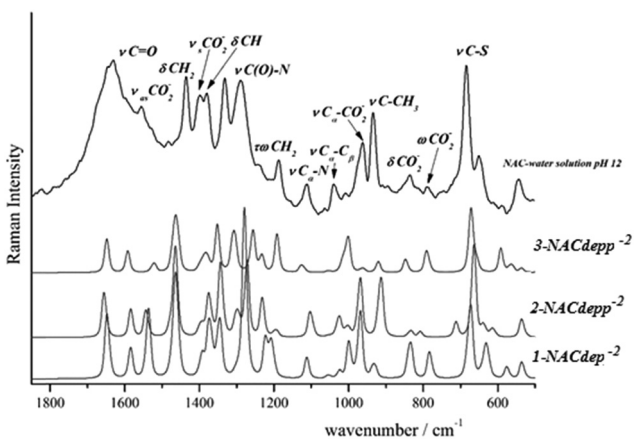

Fig. 10 The Raman spectrum of a NAC saturated solution (1 M) to pH 12, and the Raman spectra calculated with B3LYP/6-311++G(d,p).

The different pK′ values, 8.30 for Cys and 9.54 for NAC, mean that 11% of the cysteine is a thiolate at pH = 7.4, while for

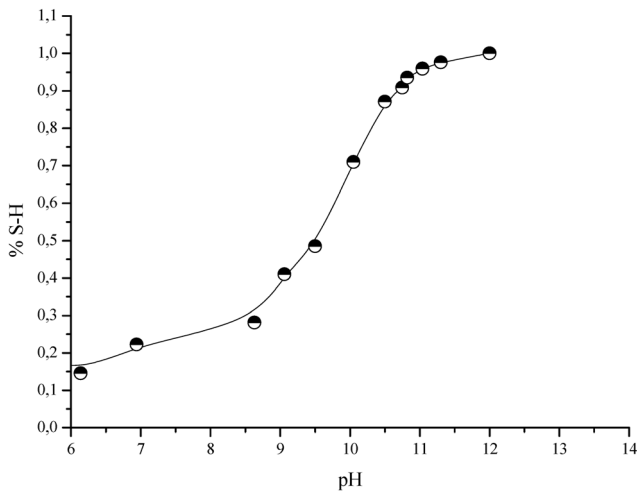

Fig. 11 Fractional ionization α_{SH} as a function of pH.

NAC only 2.5% of the NAC is a thiolate at a physiological pH. The groups that remove Cα-bound electrons, such as the carboxylate anion and the amide group, increase the acidity of the thiol site, but in this case the incorporation of the acetyl amide group decreases the acidity of the thiol group. This property accounts for the biochemical differences between Cys and NAC, in particular the antioxidant and reducing properties. The lower acidity of the SH group of NAC on the one hand makes it more resistant to air oxidation but less potent as a direct oxidant, and on the other hand it explains the greater disulphide reducing ability of NAC compared with Cys.

3.4 UV-circular dichroism spectroscopy

UV and CD data for NAC at different pH of water solutions were measured at 298 K. NAC has an absorption maximum, in aqueous solution, at 228, 232 and 240 nm for pH 3.28, 8.50 and 11.50 respectively (Fig. 12), while L-cysteine[39] and ethyl cysteine (CE)[40–47] show absorption maxima at 199 and 219 nm respectively. The CD signals are negative, in contrast to the sign of the corresponding L-cysteine and CE experimental CD band.

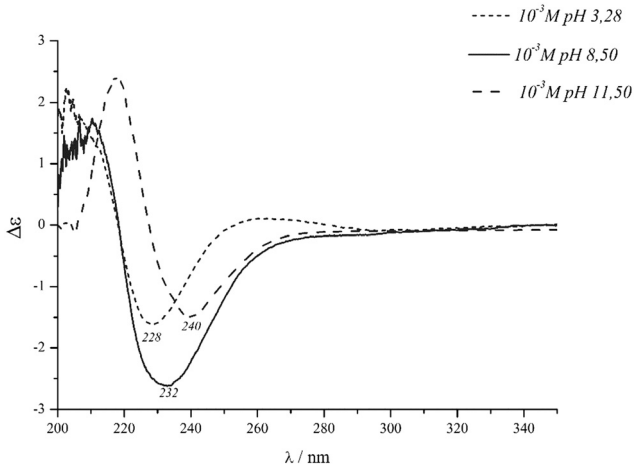

Fig. 12 UV-circular dichroism spectra of NAC in 10^{-3} M water solution at different pH.

It can be observed that as the pH increases there is an increase in λ. This is related to the fact that at pH 3, is found that the amino acid is in two forms, NAC and $NACdep^{-}$, and at pH 8 the thiol group begins to be deprotonated. At pH 11 we only see the $NACdepp^{-2}$ form. The pH effect on the Raman spectra depends on the inductive effect of the COO^{-} group on the amide and thiol groups, which is higher as the pH is raised. This can be seen in the following section of NBO analysis. This behavior is also seen in the UV spectra (Fig. 12), where it can be observed that the UV spectrum of the amino acid at pH 8 resembles that at pH 11.

Electronic excitation energies have been calculated for water solution for NAC, $NACdep^{-}$ and $NACdepp^{-2}$ at the TD-B3LYP/6-31++G(d,p) level. Note that the TD-B3LYP approach only involves the properties of the ground state, *i.e.*, the Kohn–Sham orbitals and their corresponding orbital energies obtained in a ground state calculation. Hence, excitation energies are expressed in terms of ground state properties.[48,49]

Fig. 13(A) shows the experimental UV-visible spectrum of NAC at different pH. In the spectra at pH 8 and 11, a transition to 236 nm is observed, which increases in intensity at a higher pH. This increase in the band intensity is due to the fact that at pH 8 there only exists 25% of the $NACdepp^{-2}$ form while at pH 11 the thiol group is fully deprotonated (see Fig. 11). Furthermore the maximum observed at 236 nm is produced by a π–π * transition between the S^{-} group and the amide group. This transition is sterically favorable for the 1-$NACdepp^{-2}$ form (see Fig. 13(B)). This could not be differentiated for the other degrees of dissociation because the conformer 1-$NACdepp^{-2}$ presents a greater electronic displacement with respect to the others.

3.5 NBO analysis

Table 1 shows the level of some important hyperconjugative interactions that result from the NBO analysis for the most stable conformers of NAC, $NACdep^{-}$ and $NACdepp^{-2}$, at the B3LYP/6-311+G(d) level.

The electronic charges transferred to the amide group are: $NACdepp^{-2}$ (560.34 kJ); $NACdep^{-}$ (410.61 kJ); and NAC (431.59 kJ). This fact is due to the different energy interactions between the

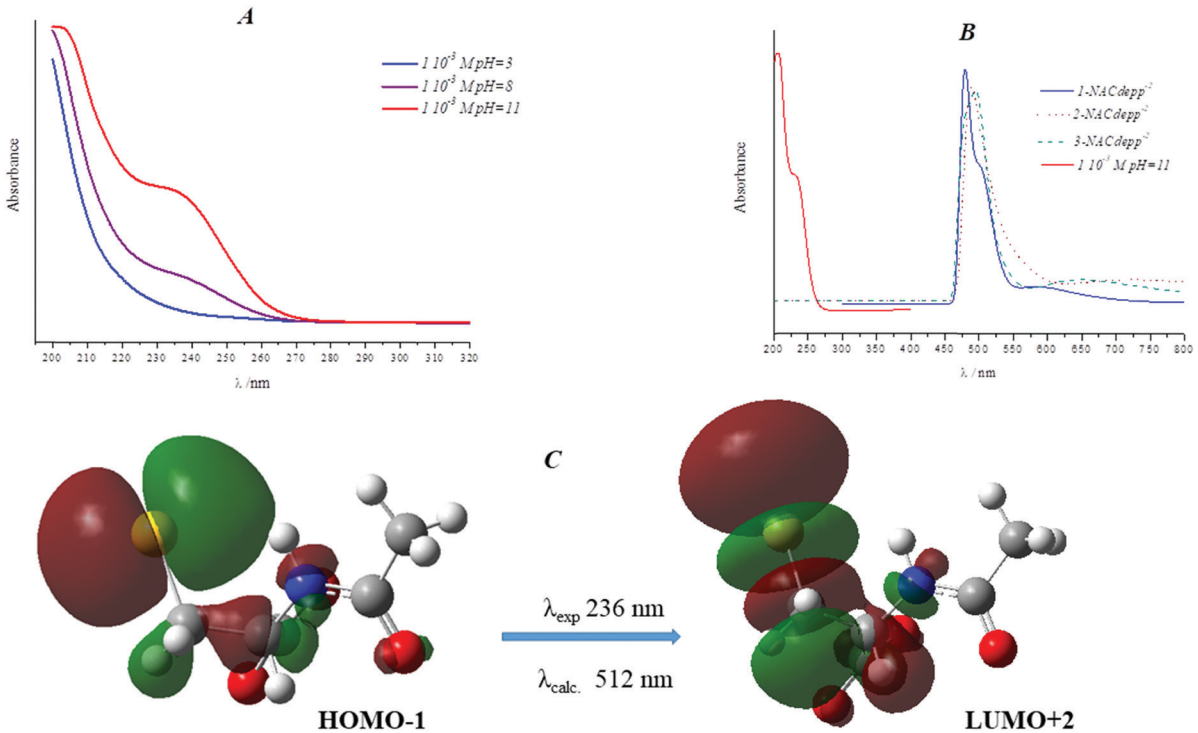

Fig. 13 (A) UV-visible spectrum at different pH values for the water solution of NAC; (B) UV-visible at pH 11 and UV-visible theoretical spectra for $NACdepp^{-2}$; and (C) the shape of HOMO–1 and LUMO+2 orbitals from TD-B3LYP/6-311G(d,p) calculations.

Table 1 Relevant hyperconjugative interactions (kJ mol^{-1}) for NAC[a,b]

	1-NAC (29%)	1-NACdep$^-$ (76%)	3-NACdepp^{-2} (42%)
LP σO1→			
σ*C2–N	6.31	7.27	7.18
σ*C1–C2	8.74	8.90	8.86
LP πO1→			
σ*C2–N	99.57	91.75	83.64
σ*C1–C2	76.08	79.67	81.00
LP σ N→			
σ*C2═O1	10.32	17.39	—
π*C2═O1	178.61	167.79	334.02
σ*Cα–C3	37.08	12.00	33.11
σ*Cα–H	3.34	3.80	7.73
σ*Cα–Cβ	11.54	22.24	5.10
LP σ O2→		—	—
σ*Cα–C3	8.94	8.24	7.06
σ*C3═O3	6.73	9.66	11.24
LP πO2→			
σ*N–Cα	—	6.10	6.81
σ*Cα–C3	81.55	77.50	70.18
σ*C3═O3	136.23	510.63	497.17
LP σ O3→			
σ*C3═O2	31.18	11.62	12.33
σ*Cα-C3	—	7.44	7.27
LP πO3→			
π*C3═O2	187.22	81.68	76.62
σ*Cα–C3	—	76.20	80.47
LP σ S→			
σ*Cα–Cβ	—	—	2.72
LP πS→			
σ*Cα–Cβ	—	16.09	21.90
σ*N–H	—	—	17.26

[a] LP denotes an electron lone pair on the atom (for atom numbering see Fig. 1). [b] Calculated at the B3LYP/6-311+G(d) level.

following orbitals: LP πO1 → σ*C2–N and LP σN → π* C2═O1 (LP: lone pair).

It is worth observing the behavior of the C2–N bond with the delocalization effect; as shown in Fig. 14, as the pH increases the hyperconjugative interaction of this bond decreases in the same way as it does for νCN (Fig. S7, ESI†). The way in which the LP πO1 → σ*C2–N interaction and νCN decrease is an inverse reflection of the fractional ionization α_{SH} (Fig. 14). This is in agreement with the calculated N–H bond length,

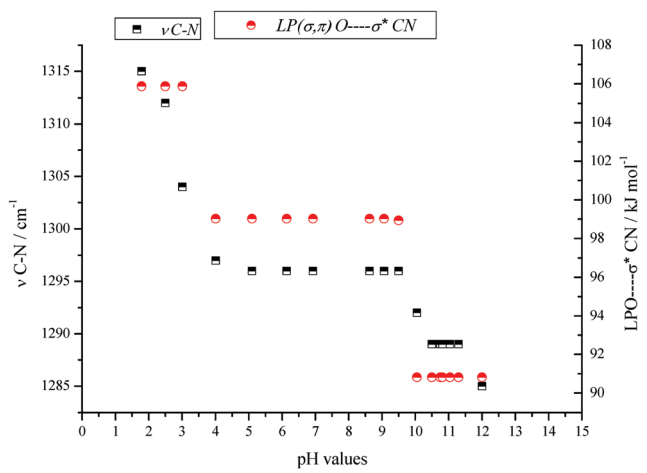

Fig. 14 Variation of νC(O)–N as a function of pH (black) and variation of νC(O)–N as a function of the interaction LPO(σ,π) → σ*C(O)–N (red).

which increases from 1.230 Å in NAC to 1.238 Å and 1.240 Å in NACdep$^-$ and NACdepp^{-2}, respectively. This causes the σ*N–H population to increase (NAC (0.018) > NACdep$^-$ (0.028) > NACdepp^{-2} (0.043)) (see Table S10, ESI†).

The delocalization of the CO_2^- group is presented at a higher degree for NACdep$^-$ than NACdepp^{-2} because of the mesomeric effect of the LP πO2 → σ*C3═O3.

The behavior of the LP π S is different for the different ionization states of NAC. It can be seen that when NAC is in the acid form, no delocalization of it is observed. Thus, while when deprotonation of the carboxylic group of NAC occurs, an anomeric effect takes place towards the neighboring σ*C_α–C_β, thus causing a decrease in the C–S bond distance (Tables S2–S5, ESI†) with an increase in the population of σ*C–S (Table S10, ESI†). Conversely, when NAC is found as a thiolate, the delocalization of the LP π S to the neighboring σ*C_α–C_β increases, while a strong hydrogen bond with the H of the amide group is formed. If we compare the behavior of the LP S of NAC with those of etylcysteine,[40] we see that the introduction of the amide group in the cysteine structure increases the acidity of the thiol site, decreasing the availability of the sulfur-free pairs.

4. Conclusions

Raman spectra of *N*-acetyl-L-cysteine in aqueous solution at different concentrations and pH were discussed and compared with theoretical calculations of electronic and vibrational structure. A detailed assignment of the most important reactive groups of the amino acid at different pH is presented. The SH dissociation constant was calculated from spectroscopic measurements of the Raman spectra.

Cysteine has a pK_a of 8.3 at 25 °C, which means that 11% of cysteine is a thiolate at pH 7.4. In contrast, NAC displays a higher pK_a value (9.5), in such a way that at pH 7.4 only 2.5% of the NAC molecules are found in the thiolate form. This difference implies a decrease in the availability of the SH group. This behavior accounts for the marked biochemical differences between Cys and NAC, in particular the antioxidant and reducing properties. The lower acidity of the SH group of NAC means that it is more resistant to air oxidation but less potent as a direct oxidant. Additionally this fact accounts for the greater disulphide reducing ability of NAC compared with Cys.

The presence of the carboxyl group in cysteine and NAC results in an increase in the amino acid acidity because the inductive effect of the carboxyl group exceeds the electrostatic effect of the negative charge. This causes ionization of the amino group within the same range as that of –SH, implying a similar pK_a. In this case, when NAC has a bonded amide on Cα, there is competition in the ionization and the thiol acidity decreases while that of the amide increases. This can be seen in the NBO results where the greatest relocation is towards the amide group.

SERS spectra indicate that the S atom is interacting with the surface through the sulfur atom. One of the consequences of the interaction with the surface is the deprotonation of the SH group, as revealed by the disappearance of the ν(S–H) band. The

calculations performed for the Ag–NAC complex confirm the experimental data obtained by SERS, where the S–Ag interaction is the most important. These results can be of great interest for drug delivery strategies where NAC is immobilized on silver nanoparticles as carriers. Raman was performed to compare the behavior of different functional groups in the molecule, both in the solid phase and in aqueous solution at different pH.

The frequency of the S–H stretching mode was seen to undergo a clear shift to higher frequencies in aqueous solution as compared to the solid. This is due to the fact that water solvation disrupts the weak S–H···NH bond found in the solid, giving rise to a strengthened S–H bond.

Finally, it is important to note that for the 1-NACdepp^{-2} form it was only possible to identify it by comparison of the theoretical and experimental UV-visible spectra.

Conflicts of interest

There are no conflicts to declare.

Acknowledgements

We thank PIUNT (D542/2), CONICET (PIP 002 and 1529) and PICT2013-0697 of R. Argentina for the research grants. We also thank MINECO grant FIS2017-84318-R.

References

1 P. C. Jocelyn, *Biochemistry of the SH Group*, Academic Press Inc, 1972.
2 M. Friedman, *The Chemistry and Biochemistry of Sulfhydryl Groups in Amino Acids, Peptides and Proteins*, Pergamon Press, New York, 1973.
3 O. I. Aruoma, B. Halliwell, B. M. Hoey and J. Butler, *Free Radical Biol. Med.*, 1989, **6**, 593–597.
4 Y. Xu, X. Y. Hou and Y. Y. Zong, *J. Neurosci. Res.*, 2009, **87**(4), 918–927.
5 A. Kamboj, R. Kiran and R. Sandhir, *Mol. Cell. Biochem.*, 2006, **286**, 107–114.
6 S. Shadnia, M. Dasgar, S. Taghikhami, A. Mohammadirad, R. Khorasani and M. Abdollahi, *Toxicol. Mech. Methods*, 2007, **17**(2), 109–115.
7 O. Pechanova, J. Kunes, Z. Dobesova, S. Vrankova and J. Zicha, *J. Physiol. Pharmacol.*, 2009, **60**(40), 21–25.
8 Y. Yurumez, M. Cemek, Y. Yavuz, Y. O. Birdane and M. E. Buyukokuroglu, *Biol. Pharm. Bull.*, 2007, **30**(3), 490–494.
9 A. L. Villalobos and R. Q. Hernández, *Revista médica de Costa Rica y Centroamérica lxiv*, 2007, vol. 57, pp. 63–69.
10 R. Mehran and A. Caixeta, *Rev. Esp. Cardiol.*, 2010, **63**(01), 9–11.
11 M. Martínez Sarrasague, D. Andrés Barrado, M. Zubillaga, A. Hager, T. De Paoli and J. Boccio, *Rev. Esp. Cardiol.*, 2006, **40**(1), 45–54.
12 A. Eftekhari, E. Ahmadian, Y. Azarmi, A. Parvizpur, H. Hamishehkar and M. A. Eghbal, *Toxicol. Mech. Methods*, 2016, **26**(7), 520–528.
13 S. Mostafalou, M. Abdollahi, M. A. Eghbal and N. S. Kouzehkonani, *Adv. Pharm. Bull.*, 2012, **2**(1), 79–88.
14 F. Takusagawa, T. F. Koetzle, W. W. H. Kou and R. Parthasarathy, *Acta Crystallogr., Sect. B: Struct. Crystallogr. Cryst. Chem.*, 1981, **37**, 1591–1596.
15 B. Boeckx, R. Ramaekers and G. Maes, *J. Mol. Spectrosc.*, 2010, **26**, 73–81.
16 M. Reza Poopari, Z. Dezhahang and Y. Xu, *Spectrochim. Acta, Part A*, 2015, **136**, 131–140.
17 R. Cecil, In *The Proteins*, ed. H. Neurath, Academic Press Inc., New York, 2nd edn, 1963.
18 D. Garfinkel and J. T. Edsall, *J. Am. Chem. Soc.*, 1958, **80**, 3823–3826.
19 E. L. Elson and J. T. Edsall, *Biochemistry*, 1962, **1**, 1–7.
20 J. Tomasi and M. Persico, *Chem. Rev.*, 1994, **94**, 2027–2094.
21 J. Tomasi, B. Mennucci and R. Cammi, *Chem. Rev.*, 2005, **105**, 2999–3093.
22 C. J. Cramer and D. G. Truhlar, *Acc. Chem. Res.*, 2008, **41**, 760–768.
23 K. H. Hopmann, K. Ruud, M. Pecul, A. Kudelski, M. Dracinsky and P. Bour, *J. Phys. Chem. B*, 2011, **115**, 4128–4137.
24 J. Kubelka, R. Huang and T. A. Keiderling, *J. Phys. Chem. B*, 2005, **109**, 8231–8243.
25 J. P. Foster and F. Weinhold, *J. Am. Chem. Soc.*, 1980, **102**, 7211–7218.
26 A. E. Reed, R. B. Weinstock and F. Weinhold, *J. Chem. Phys.*, 1985, **83**, 735–746.
27 M. V. Cañamares, J. V. Garcia-Ramos, J. D. Gomez-Varga, C. Domingo and S. Sanchez-Cortes, *Langmuir*, 2005, **21**, 8546–8553.
28 M. J. Frisch Trucks, H. B. Schlegel, G. E. Scuseria, M. A. Robb, J. R. Cheeseman, J. A. Montgomery Jr., T. Vreven, K. N. Kudin and J. C. Burant, *et al.*, *Gaussian 03 (Revision D.01)*, Gaussian, Inc., Wallingford, CT, 2004.
29 M. J. Frisch, *et al.*, *Gaussian 09, Revision B.01*, Gaussian, Inc., Wallingford, CT, USA, 2009.
30 A. D. Becke, *J. Chem. Phys.*, 1993, **98**, 5648.
31 C. Lee, W. Yang and R. G. Parr, *Phys. Rev. B: Condens. Matter Mater. Phys.*, 1988, **37**, 785–789.
32 S. Miertuš, E. Scrocco and J. Tomasi, *Chem. Phys.*, 1981, **55**, 117–129.
33 (*a*) P. J. Hay and W. R. Wadt, *Ab initio* effective core potentials for molecular calculations. Potentials for the transition metal atoms Sc to Hg, *J. Chem. Phys.*, 1985, **270**, 270; (*b*) P. J. Hay and W. R. Wadt, *Ab initio* effective core potentials for molecular calculations. Potentials for main group elements Na to Bi, *J. Chem. Phys.*, 1985, **82**, 284; (*c*) P. J. Hay and W. R. Wadt, Ab initio effective core potentials for molecular calculations. Potentials for K to Au including the outermost core orbitals, *J. Chem. Phys.*, 1985, **82**, 299.
34 A. D. McLean and G. S. Chandler, Contracted Gaussian basis sets for molecular calculations. I. Second row atoms, $Z = 11–18$, *J. Chem. Phys.*, 1980, **72**, 5639–5648.
35 R. Krishnan, J. S. Binkley, R. Seeger and J. A. Pople, Self-consistent molecular orbital methods. XX. A basis set for correlated wave functions, *J. Chem. Phys.*, 1980, **72**, 650–654.

36 B. Nielsen and A. J. Holder, *GaussView, User's Reference*, Gaussian Inc., Pittsburgh, PA, 1997–1998.
37 D. Glendening, J. K. Badenhoop, A. D. Reed, J. E. Carpenter and F. F. Weinhold, *NBO 4.0 E*, Theoretical Chemistry Institute, University of Wisconsin, Madison, WI, 1996.
38 M. R. Poopari, Z. Dezhahang, G. Yang and Y. Xu, *ChemPhysChem*, 2012, **13**(9), 2310–2311.
39 P. G. Jonsson and A. Kvlck, *Acta Crystallogr., Sect. A: Cryst. Phys., Diffr., Theor. Gen. Crystallogr.*, 1972, **28**, 1827–1833.
40 M. E. Defonsi Lestard, S. B. Díaz, M. Puiatti, G. A. Echeverría, O. E. Piro, A. B. Pierini, A. Ben Altabef and M. E. Tuttolomondo, *J. Phys. Chem. A*, 2013, **117**, 14243–14252.
41 E. López-Tobar, B. Hernández, M. Ghomi and S. Sanchez-Cortes, *J. Phys. Chem. C*, 2013, **117**, 1531–1537.
42 M. Kaminski, A. Kudelski and M. Pecul, *J. Phys. Chem. B*, 2012, **116**, 4976–4990.
43 P. Bazylewski, R. Divigalpitiya and G. Fanchini, *RSC Adv.*, 2017, **7**, 2964–2970.
44 NIST Critically Selected Stability Constants of Metal Complexes Database.
45 R. E. Benesch and R. Benesch, *J. Am. Chem. Soc.*, 1955, **77**, 5877–5881.
46 D. M. E. Reuben and T. C. Bruice, *J. Am. Chem. Soc.*, 1976, **98**, 114–121.
47 L. Fowden, P. M. Scopes and R. N. Thomas, *J. Chem. Soc.*, 1971, 833–840.
48 W. Koch and M. C. Holthausen, *A Chemist's Guide to Density Functional Theory*, Wiley-VCH, Weinheim, 2nd edn, 2001.
49 G. R. Hutchison, Y. J. Zhao, B. Delley, A. J. Freeman, M. A. Ratner and T. Marks, *Phys. Rev. B: Condens. Matter Mater. Phys.*, 2003, **68**, 035204.

